

Supplementary Information for

Energy-dependent quenching adjusts the excitation diffusion length to regulate photosynthetic light harvesting

Doran I.G. Bennett, Graham R. Fleming and Kapil Amarnath

Corresponding Authors.

E-mail: doranbennett@g.harvard.edu, grfleming@lbl.gov, kapil@alum.mit.edu

This PDF file includes:

Supplementary text
Figs. S1 to S5
Table S1
References for SI reference citations

Supporting information materials and methods

Overview of multiscale model. We generated membranes with different organizations of PSII supercomplexes and LHCII using Monte Carlo simulations of a 200 nm x 200 nm area containing coarse-grained PSII supercomplex (pill) and LHCII particles (circle) (Main text, Fig. 1B) (1). We superimposed the crystal structures of the chlorophyll pigments of the C₂S₂ PSII supercomplex (2) and LHCII (3) to establish the locations of all pigments in the membrane. We assumed random orientations of the LHCII. The Monte Carlo simulations allow for the energetic attachment of LHCII to the PSII supercomplexes in the location where the so-called ‘medium-bound’ LHCII can bind, which results in the largest stable form of the PSII supercomplex in plants, the C₂S₂M₂ supercomplex (4). We have not included CP24, and the minor complexes are modeled as LHCII monomers, since the crystal structures of CP24 and CP26 are still lacking.

Excitation energy transport rates between domains of strongly coupled chlorophyll (~3-4 pigments in size) were calculated using Generalized Förster theory assuming that excitations thermalize within domains prior to hopping between domains. A quantum-mechanically exact calculation of energy transfer for a system of the size of the thylakoid membrane (~50,000 pigments) is currently infeasible. Computationally more tractable perturbative methods include modified Redfield theory, in which interactions between electronic states and the vibrational modes of the system are perturbative, and Generalized Förster theory, in which the electronic coupling between pigments is perturbative (5). The pigment-protein complexes that compose PSII do not lie on either of these extremes, so Renger (6) and Novoderezhkin (7) pioneered an approach in which pigments are grouped into domains within which transport can be described by Modified Redfield theory, and between which transport is described by Generalized Förster theory (8, 9). We defined domains to maximize the separation of timescales between intra- and inter-domain transfer (10). We can assume instantaneous equilibration within a domain without loss of accuracy in our simulations; however, the domain picture is the most coarse-grained picture that reproduces the dynamics of transport (10). The domains for a monomer of the LHCII trimer are color-coded in the crystal structure in the main text (Main text, Fig. 1C). The rate of transport between two domains, a donor d and an acceptor a , is the Boltzmann-weighted sum of the rates of transport between each pair of excitons in the two domains ($|M\rangle$ and $|N\rangle$, respectively):

$$k_{a\leftarrow d}^{\text{dom}} = \sum_{\substack{|M\rangle \in d \\ |N\rangle \in a}} k_{N\leftarrow M} P_M^{(d)}, \quad [1]$$

where $P_M^{(d)} = \frac{e^{-E_M/k_B T}}{\sum_{|M\rangle \in d} e^{-E_M/k_B T}}$. The rate between two excitons was calculated using Generalized Förster theory,

$$k_{N\leftarrow M} = \frac{|V_{M,N}|^2}{\hbar^2 \pi} \int_0^\infty dt A_N(t) F_M^*(t), \quad [2]$$

where $|V_{M,N}|^2$ is the electronic coupling between the two excitons and $\int_0^\infty dt A_M(t) F_N^*(t)$ is the overlap integral between the normalized absorption lineshape of the acceptor and fluorescence lineshape of the donor. This model of excitation transport shows good agreement with more exact methods for simulating the excitation population dynamics (11, 12). Here we inhomogeneously average the rates of transport before calculating the dynamics, which offers substantial computational savings and does not affect excitation dynamics (13).

Previously, we noticed that when embedding the crystal structures into the coarse-grained Monte Carlo simulation pigments belonging to adjacent proteins would occasionally be unphysically close (Ref. (13), see Supplementary Text) resulting in transport rates that were many orders of magnitude faster than any other rates in the network. These unphysically high rates of transport meant numerical propagation of exciton dynamics required extremely fine time steps. To reduce computational expense, we additionally lowered any rate constants greater than 2 ps⁻¹, which arise due to imperfect overlay of the pigments on the Monte Carlo simulations (13), to 2 ps⁻¹. We found that this does not influence the simulated photochemical yield or fluorescence decay (13) but greatly simplified the simulations.

We modeled electron transfer using a simple phenomenological kinetic model with three rate constants that describe both reversible and irreversible charge separated states:



Here, RC is the reaction center domain composed of the 8 central pigments of the reaction center. The ‘‘radical pair’’ states RP1 and RP2 and the rate constants k_{RC} , k_{CS} , and k_{irr} are used to model the electron transfer steps in the reaction center. RP1 and RP2 are non-emissive states that do not necessarily have a direct physical analog with charge-separated states in the reaction center. Rather, this approach allows us to describe the overall process of a reversible charge separation step followed by an irreversible step and establish the approximate timescales of these events relative to energy transfer in the light harvesting antenna. The rates were previously parameterized using fluorescence decays of PSII supercomplexes of different sizes (14), with $\tau_{CS} = 0.64$ ps, $\tau_{RC} = 160$ ps, and $\tau_{irr} = 520$ ps ($k = 1/\tau$) (10). These same three parameters can fit data from PSII

supercomplexes with a range of antenna sizes (10) and the thylakoid membrane(13) without any alteration or refitting (Main Text, Fig. 1E).

In order to simulate dynamics in the presence of closed RCs, we also need to parameterize the behavior of the charge separated (radical pair, RP) states when $k_{irr} \rightarrow 0$. In keeping with our previous work, we have used $\tau_{CS} = 310$ ps and $\tau_{RC} = 458$ ps which were previously determined by fitting to fluorescence decay data from leaves with closed RCs (13) (Main text, Fig. 1E). An alternative approach to determining these rate constants would be to fit data on isolated supercomplexes with closed RCs, analogous to what we have done to determine the open RC parameters. Unfortunately, we are not aware of any spectroscopic data taken on PSII supercomplexes other than the core complex (15) when RCs are closed. We find, however, the τ_{CS} and τ_{RC} that best fit the isolated core complex data ($\tau_{CS} = 125$ ps and $\tau_{RC} = 6.25$ ns, Fig. S4A) does not provide a good description of the fluorescence decay data from leaves with closed RCs (Fig. S4B). We note that this inconsistency between core complex data and the membrane measurements is not unexpected; we previously found a similar inconsistency between the open reaction center core complex data and larger PSII supercomplexes (10) as well as the membrane data (13). However, open RC models for measurements of the larger PSII supercomplexes and the membranes were themselves consistent - thus suggesting that directly fitting the charge separation model on the membrane may provide a reasonable description of the charge separation timescales for closed RCs in the absence of larger PSII supercomplex measurements. We further note that the physical mechanisms described in the current work should not change as a result of reparametrizing the closed RCs to agree with the isolated core complex measurements since they would be the equivalent of a very low-density, weak quencher.

The overall picture of PSII light harvesting from our model is as follows. The nodes of the energy transfer network are domains of ~ 3 -4 tightly coupled chlorophylls. In the absence of qE, excitation are dissipated by fluorescence (Φ_{F1}), non-radiative decay (Φ_{NR}), and productive charge separation at an open RC (Φ_{PC}). While every domain can dissipate excitation by fluorescence (average timescale $\tau_{F1} = 16$ ns) or non-radiative decay ($\tau_{nr} = 2$ ns), only the open reaction centers perform irreversible charge separation. When qE is active, excitations at a qE quenching site are dissipated (timescale τ_{qE}) resulting in a qE yield (Φ_{qE}), as well.

Monte Carlo Simulations. On a given membrane, a kinetic Monte Carlo scheme was also used to determine the yields of the different decay pathways using 5,000 trajectories with an initial domain sampled with a probability proportional to the number of ChlA in the domain. Kinetic Monte Carlo was also used to calculate the diffusion length scale. In this case, the simulation is done in two steps. First the one-over-e time - the time at which the fraction of the unquenched excitation becomes equal to e^{-1} - is calculated. Then the average absolute displacement from the initial domain at the one-over-e time is calculated for 5,000 trajectories. For L_D calculations, the ChlA initial condition is modified to only allow excitation starting in 40 nm x 40 nm patch at the center of the membrane to ensure minimal effects from the boundaries of the membrane.

Fluorescence lifetime snapshot data analysis. Fluorescence lifetime snapshots were measured during the application of a dark-light-dark actinic light sequence on dark-adapted wild-type leaves of *A. thaliana* (16). The light period was 10 min, with an actinic light intensity of 1200 $\mu\text{mol photons m}^{-2} \text{s}^{-1}$. The snapshots were taken under light conditions in which the reaction centers were closed. Each lifetime was fit to a sum of three exponential decays, such that the sum of the amplitudes of each decay was normalized to 1. The shortest decay had a time constant that varied between 65 and 85 ps, the middle decay had a time constant that varied between 480 and 1020 ps, and the longest decay had a time constant that varied between 1.2 and 2.3 ns. The amplitude of the shortest component before actinic light exposure was taken to be the photosystem I (PSI) contribution to all decays. At this time point we assumed no NPQ had turned on and that the only contribution to the shortest lifetime component was from PSI (17). This PSI amplitude was subtracted from the amplitude of shortest decay component at all other time points, since we assume that the PSI contribution to the lifetime does not change during the actinic light sequence. The amplitudes at each time point were then renormalized to sum to 1, resulting in the PSII component of the fluorescence lifetime. Fig. 2A of the main text indicates the average lifetime of PSII component over the course of the the dark-light-dark sequence. Fig. 2B of the main text (dotted lines) indicates the PSII component of the fluorescence lifetime.

In Fig. 2B, Fig. 2E, and Fig. 2F of the main text we plot the fluorescence lifetimes simulated with our multiscale model with a particular combination of a timescale of quenching τ_{qE} and a probability of activation of P_{qE} that gave best agreement with fluorescence lifetime snapshot data. We calculated the amplitude-weighted error between our simulation ($F_{\text{model}}(t; f_{RC} = 0, k_{qE}, P_{qE})$) and the data ($F_{\text{data}}(t; T)$):

$$\text{Amplitude Weighted Error} = \sum_t F_{\text{data}}(t; T = 6.5 \text{ min}) (F_{\text{model}}(t; f_{RC} = 0, \tau_{qE}, P_{qE}) - F_{\text{data}}(t; T))^2. \quad [4]$$

We determined the areas indicated in Fig. S1A and Fig. S4 using the amplitude-weighted error and also a yield ratio error,

$$\text{Yield Ratio Error} = \text{abs} \left(\frac{\sum_t F_{\text{data}}(t, T = 6.5 \text{ min})}{\sum_t F_{\text{data}}(t, T = -2 \text{ min})} - \frac{\Phi_{F1, \text{model}}(f_{RC} = 0, \tau_{qE}, P_{qE})}{\Phi_{F1, \text{model}}(P_{\text{open}} = 0, k_{qE} = 1/\tau_{qE} = 0)} \right). \quad [5]$$

The areas indicate (τ_{qE}, P_{qE}) combinations that result in an amplitude weighted error less than 0.30 and a yield ratio error less than 0.15. We calculated the error for each combination of $P_{qE} = 0 : 0.05 : 1$ and $k_{qE} = 1/\tau_{qE} = 0 : 0.005 : 0.1 \text{ ps}^{-1}$ and interpolated intermediate values.

Calculation of pulse-amplitude-modulated (PAM) chlorophyll fluorescence parameters from multiscale simulations. Pulsed-amplitude-modulated (PAM) fluorescence is extensively used to characterize photosystem II function in leaves (18–21). The method measures the relative changes in chlorophyll fluorescence yield of PSII as it is exposed to both changes in actinic light intensity that activate qE and periodic short (<1 s) saturating pulses of light that close all reaction centers. In this work, we use the fluorescence yields simulated using the multiscale model for PSII light harvesting to calculate parameters from a PAM measurement.

The main chlorophyll fluorescence parameters are as follows:

- F_m : Φ_{F1} with no qE activated and all RCs closed
- F_m' : Φ_{F1} with qE activated and all RCs closed
- F_s : Φ_{F1} with qE activated and some fraction of reaction centers open
- F_o' : Φ_{F1} with qE activated and all reaction centers open

Using our bottom-up multiscale model we can directly calculate the photochemical yield (Φ_{PC}) as a function of arbitrary sites of qE, different levels of qE activation (given by the timescale of quenching τ_{qE} and the probability of qE activation P_{qE}), and different fractions of open reaction centers (f_{RC}). To compare simulations using our model to the predictions of the lake and puddle models, we calculated the chlorophyll fluorescence parameters from PAM fluorescence listed above from the corresponding fluorescence yields calculated with our simulations. The fluorescence yield Φ_{F1} depends on the levels of qE (i.e. the excitation diffusion length - L_D) and the fraction of open RCs (f_{RC}). The L_D is 50.4 nm with no qE active, and less than 50.4 nm if any qE is active.

We calculated the fraction of open reaction centers predicted by the lake (q_L , Fig. 4B, Fig. S3B) and puddle (q_P , Fig. S3B) models as follows:

$$q_P = \frac{F_m' - F_s}{F_m' - F_o'} = \frac{\Phi_{F1}(L_D, f_{RC} = 0) - \Phi_{F1}(L_D, f_{RC})}{\Phi_{F1}(L_D, f_{RC} = 0) - \Phi_{F1}(L_D, f_{RC} = 1)} \quad [6]$$

$$q_L = q_P \frac{F_o'}{F_s} = q_P \frac{\Phi_{F1}(L_D, f_{RC} = 1)}{\Phi_{F1}(L_D, f_{RC})} \quad [7]$$

We calculated photochemical yield as predicted by the lake and puddle models, the Φ_{II} parameter (22), as follows:

$$\Phi_{PC}^{F1}(L_D, f_{RC}) = \frac{\Phi_{F1}(L_D, f_{RC} = 0) - \Phi_{F1}(L_D, f_{RC})}{\Phi_{F1}(L_D, f_{RC} = 0)} \quad [8]$$

$$\Phi_{II} = \frac{F_m' - F_s}{F_m'}$$

Lastly, we calculated the NPQ parameter, which is used to measure the extent of activation of any NPQ mechanisms including qE, as follows:

$$NPQ(L_D) = \frac{\Phi_{F1}(L_D = 50.4 \text{ nm}, f_{RC} = 0) - \Phi_{F1}(L_D, f_{RC} = 0)}{\Phi_{F1}(L_D, f_{RC} = 0)} = \frac{F_m - F_m'}{F_m'} \quad [9]$$

Supporting Information Text

Weak quenchers in the presence of open reaction centers. We have shown in the main text that the influence of a spatially uniform distribution of weak quenchers on excitation transport in PSII is to reduce the excitation diffusion length (L_D) and this holds for different qE parameters and different sites of quenching. We find the same simplification holds when both qE and open RCs are present (Fig. S1B). For both LHCII-610 and LHCII-608, the spatial distribution of quenchers is uncorrelated with open RCs and homogeneously distributed over the PSII enriched portion of the thylakoid membrane. Fig. S1B shows that at a fixed excitation diffusion length (L_D) the photochemical yield as a function of the fraction of open RCs is identical for LHCII-610 (blue solid line) and LHCII-608 (green dashed line). At low fraction of open RCs, mLHC-610 (purple dashed line) also shows identical behavior but deviates slightly with increasing fraction of open RCs. Unlike LHCII-610 and LHCII-608, mLHC-610 arises only in the PSII supercomplexes and therefore co-localizes with RCs. At low fraction of open RCs, this results in only a weak correlation because most mLHC-610 sites will co-localize with closed RCs leading to an effectively uncorrelated spatial distribution of quenchers and open RCs. With the fraction of open reaction centers equal to 1, however, every mLHC-610 site is co-localized with an open RC. Since RCs act as strong quenchers and qE sites are weak quenchers, the resulting competition between quenchers is slightly more favorable for open RCs, leading to the approximate 10% increase in photochemical yield for mLHC-610 quenching sites.

Coarse-grained models of PSII light harvesting: Lake and Puddle. The lake and puddle models have been widely used since the 1960s (23, 24) to describe PSII light harvesting in the presence of qE, but they coarse-grain over the spatial aspects of competition. In particular, both models assume that the fraction of excitation available to reaction centers is the same as qE activates (i.e. the excitation diffusion length L_D is independent of qE). The lake and puddle models differ, however, in their assumptions about the form of competition between reaction centers. The lake model assumes simple kinetic competition between photochemistry, qE, and intrinsic decay pathways such as fluorescence and intersystem crossing for a single pool of chlorophyll excitations. The puddle model, however, assumes that this kinetic competition occurs separately for each reaction center and its associated antenna.

Here we explore the extent to which the lake and puddles models can reproduce the relationship between chlorophyll fluorescence, photochemical yield, and fraction open reaction centers simulated with our multiscale model. Since the relationship between the lake/puddle model parameters and the kinetic rate matrix underlying our multiscale model is not clear, in the following, we will combine chlorophyll fluorescence simulated with the multiscale model of PSII with PAM parameters (see ‘Calculation of PAM chlorophyll fluorescence parameters from multiscale simulations’ section above) to calculate the average RC antenna size (Fig. S2A), the fraction of open RCs (Fig. S2B), and the photochemical yield (Fig. S3A) determined by the lake and puddle models. These results assess the extent to which the lake and puddle models can recapitulate the multiscale simulation.

The average open reaction center antenna size (σ_{PC}) provides a useful measure of the connection between the photochemical yield and the fraction of open reaction centers. We simulate the average open RC antenna size (σ_{PC}) in the lake and puddle models by combining the definitions for the photochemical yield predicted by the lake and puddle models (Φ_{II}) described in ref. (22) with eq. 1 from the Main Text. For the lake model, we find

$$\sigma_{PC} = \left(\frac{k_{PC}}{k_{F1} + k_{nr} + k_{qE} + f_{RC}k_{PC}} \right) \frac{N_{ChlA}}{N_{RC}}, \quad [10]$$

where k_{PC} , k_{F1} , k_{nr} , and k_{qE} are effective rate constants for photochemistry, fluorescence, non-radiative decay, and qE quenching, respectively. Here, because of perfect competition between open RCs, σ_{PC} goes as $\sim 1/f_{RC}$ (red dashed line, Fig. S2A). Overall, the lake model (Fig. S2A, red dashed line) shows good agreement with the multiscale model when the excitation diffusion length is long ($L_D = 50$ nm), but overestimates the average antenna size when the diffusion length decreases. On the other hand, for the puddle model,

$$\sigma_{PC} = \left(\frac{k_{PC}}{k_{F1} + k_{nr} + k_{qE} + k_{PC}} \right) \frac{N_{ChlA}}{N_{RC}}, \quad [11]$$

which means that there is no dependence of σ_{PC} on the fraction of open reaction centers (f_{RC}), as would be expected in a model without competition between open centers (blue dashed line, Fig. S2A). Due to the absence of competition between open reaction centers, the puddle model provides a reasonable description when $L_D = 19$ nm and only a few RCs are open. Neither coarse-grained model captures the average open reaction center antenna size (σ_{PC}) in the intermediate regime ($L_D = 25$ nm) appropriate for qE in wild type *A. thaliana* exposed to $1200 \mu\text{mol photons m}^{-2} \text{s}^{-1}$ for 10 minutes (Fig. 2, Main Text).

From the perspective of analyzing PAM data, it is also useful to know how well the lake and puddle models can correctly estimate the fraction of open RCs from chlorophyll fluorescence and photochemical yield. We calculate the fraction of open RCs (f_{RC}) estimated with the lake and puddle models using the qL and qP parameters, respectively, from the PAM fluorescence literature (22). The estimated fraction of open RCs (y-axis) are plotted against the fraction of open RCs used in the multiscale simulation that generated the chlorophyll fluorescence data (x-axis) in Fig. S2B. The puddle model is found to dramatically over-estimate the fraction of open RCs (blue dots, Fig. S2B) when the excitation diffusion length is large (i.e. in the absence of qE) - a consequence of substantially underestimated the photochemical cross-section of each reaction center (Fig. S2A). The lake model provides a reasonable, if slight underestimation, for the fraction of open RCs across the range of excitation diffusion lengths studied here (red dots, Fig. S2B).

The photochemical yield estimated from chlorophyll fluorescence is the same for the lake and puddle model (Φ_{II}). In Fig. S3A, we compare Φ_{II} calculated from chlorophyll fluorescence simulated with the multiscale model to the photochemical yield directly simulated from the multiscale model (Φ_{PC}). For a given excitation diffusion length (L_D), we find a linear relationship $\Phi_{PC} = m(L_D) \cdot \Phi_{II}$, with a slope ($m(L_D)$) that decreases with the excitation diffusion length. We rationalize this decrease in the slope in terms of the fraction of excitations that become inaccessible to any open RC as the excitation diffusion length decreases. It is this inaccessible fraction of excitations that neither the lake nor puddle model can correctly account for and which, therefore, limits their utility when studying chlorophyll fluorescence during qE activation. We find a simple mono-exponential curve provides a good description of the relationship between the slope ($m(L_D)$) and the excitation diffusion length (L_D), as shown in Fig. S3B. It is important to note that the results in Fig. S3B represent a numeric interpolation and as such cannot be trusted outside of the simulated data range (NPQ parameter = 0-9 and $L_D = 50-15$ nm).

Weak quenching: evidence from single-molecule measurements. We estimate the rate of quenching appropriate to each proposed quenching site based on the observation of excitation lifetimes in single-molecule measurements of quenched supercomplexes (25). Using Monte Carlo simulations where excitations instantaneously thermalized within *protein* compartments (e.g. LHCII monomers or minor light harvesting complexes CP26/CP29), Gruber, *et al.*, isolated an effective quenching rate of 50 ps (25). Since excitations are assumed to be in equilibrium within a protein compartment, the specific identity of the quenching site (domain) will modify the underlying *domain-level* quenching rate that matches this result - i.e. a domain that

is less populated at equilibrium will require a faster qE quenching rate than its more populated counterpart to achieve the same effective quenching rate for the whole protein compartment. For the three sites of quenching considered here, we find the corresponding quenching timescales to be consistent with Gruber, *et al.*:

- LHCII-610: $\tau_{\text{qE}} = 21$ ps
- LHCII-608: $\tau_{\text{qE}} = 2$ ps
- mLHCII-610: $\tau_{\text{qE}} = 21$ ps

We note that the rate of quenching extracted from the single-molecule evidence for the LHCII-610 quenching site (~ 20 ps) matches well with semi-empirical calculations of quenching in the LHCII-610 domain by transport to the adjacent lutein ($\tau_{\text{qE}} \approx 30$ ps) (26).

Whether a particular quenching model is in the strong or weak limit is most easily determined by considering the probability that an excitation on the qE site will be lost due to quenching. For a weak quencher, an excitation on the active qE site has only a small probability of being quenched before another process occurs. We calculate the probability that an excitation on an active qE site is quenched (f_{qE}) using

$$f_{\text{qE}} = \frac{\tau_{\text{qE}}^{-1}}{\tau_{\text{qE}}^{-1} + \tau_{\text{dwell}}^{-1}}, \quad [12]$$

where τ_{qE} is the timescale of quenching from an active qE site, and τ_{dwell} is the inverse of the sum of all other rates out of the domain. We report τ_{dwell} extracted from our multiscale model in Table S1. We find that in all cases the estimated quenching timescale (τ_{qE}) is much larger than the dwell time (τ_{dwell}) and therefore we find that current single-molecule measurements suggest qE sites are weak quenchers.

Probability of the quenched conformation: evidence from single molecule data. Kruger, *et al.*, measured the chlorophyll fluorescence of isolated LHCII trimers in a variety of qE mimicking conditions (27). Based on the distribution of chlorophyll fluorescence intensities observed in each condition, the authors assigned a percentage of the time the complexes spent in a quenched state. The highest observed percentage of time that trimers were in a quenched state was $\sim 30\%$. If each of the three monomers composing the LHCII trimer contained an active qE site each time a quenched complex was observed, this percentage in time would correspond to a maximum value of P_{qE} (probability of a qE site being activated) of 30%. This value, in combination with the timescale of quenching estimated above provides a parameterization of a qE model from single molecule measurements. Our interpretation, presented in the Discussion section of the Main Text, is merely a proof of concept of how single molecule data might be related to the quenching measured on intact leaves. A more detailed analysis of the single molecule data is required for a more precise interpretation in the context of our model and PAM fluorescence data of qE mutants.

Effect of membrane organization. Further, we have considered the role of membrane organization. There have been reports of the segregation of PSII supercomplexes and LHCII during qE (28, 29), though this is not established. Fitting fluorescence lifetime data with quenching on LHCII-610 in segregated membranes results in a similar area of best-fit as for mixed membranes, but shifted to the right (Fig. S5). Despite this similarity, the spatial heterogeneity of quenchers means that the excitation diffusion length by itself is insufficient as a simplifying concept, and we do not pursue the coarse-graining of quenching in segregated membranes here.

qE site	$\tau_{\text{dwell}}^{\text{median}}$ (ps)	$\tau_{\text{dwell}}^{\text{min}}$	$\tau_{\text{dwell}}^{\text{max}}$
LHCII-610	2.7	0.21	4.30
LHCII-608	0.31	0.14	0.31
mLHC-610	2.2	0.21	4.00

Table S1. Median, minimum, and maximum dwell times in the mixed membrane for the chlorophyll domains considered as qE sites in this work: LHCII 610-612 (LHCII-610), minor LHCs 610-612 (mLHC-610), and LHCII 601,608,609 (LHCII-608). The dwell time is defined as the inverse of the sum of all rates out of a domain *except* for qE. These rates include excitation transport, fluorescence, and dumping. A distribution of dwell times arises because the excitation transport rates out of a domain depend on its position in the membrane.

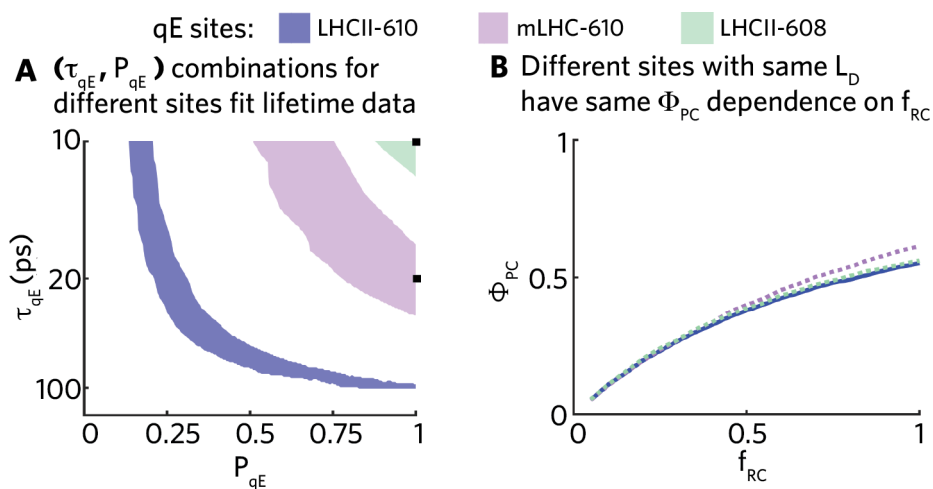


Fig. S1. Different combinations of qE parameters reproduce the same excitation diffusion length and dynamics for different qE sites. (A) The (τ_{qE}, P_{qE}) combinations that are consistent with the fluorescence lifetime data from a light acclimated leaf for different sites of quenching (Main Text, Fig. 2B, blue dotted line; see SI Methods, Fluorescence lifetime snapshot data analysis for how this was determined). These best-fit regions all share the same excitation diffusion length ($L_D = 25$ nm). The best-fit combinations for the minor light harvesting complex Chl610-612 (mLHC-610) site (light purple) are shifted to the right relative to those for LHCII-610 (blue) because there are fewer mLHCII-610 sites in the membrane, but the density of quenchers, or the number of active quenching sites per unit area, is the same. Only one (τ_{qE}, P_{qE}) combination for the LHCII Chl601,608,609 domain (LHCII-608, light blue green) has an L_D of 25 ± 2.5 nm because it contains chlorophyll *b* and has a higher effective free energy than Chl610-612. (B) The photochemical yield (Φ_{PC}) as a function of the fraction of open reaction centers (f_{RC}) is plotted for all three sites when $L_D = 25$ nm. The small variation in the values of the mLHC-610 site are explained in the accompanying text in terms of spatial correlation between quenching sites of open reaction centers.

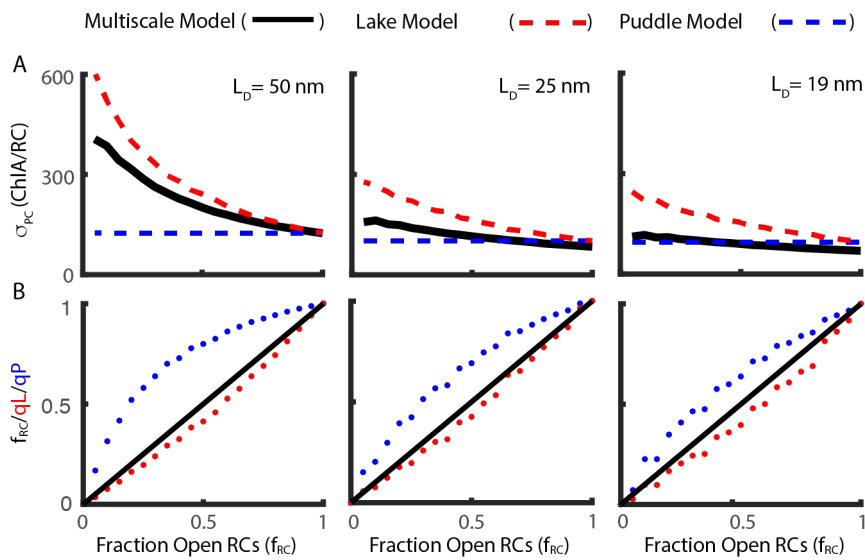


Fig. S2. Comparing the lake and puddle models to multiscale simulations. As outlined in the Supplementary Text, we determine the lake and puddle model predictions for the photochemical yield (Φ_{II}) and the fraction of open reaction centers (qL and qP) using chlorophyll fluorescence simulated with the multiscale model. The agreement with the multiscale simulation ability assesses whether the lake and puddle models accurately describe the interaction between chlorophyll fluorescence, qE, and open reaction centers. **(A)** The lake (red dashed line) and puddle (blue dashed line) model prediction for the average open reaction center antenna size (σ_{RC}) is plotted as a function of the fraction of open reaction centers in the multiscale simulations when the excitation diffusion length (L_D) is 50 nm (left panel), 25 nm (middle panel), and 19 nm (right panel). These results are compared to the results of the multiscale simulation (black line). **(B)** The lake (red dots) and puddle (blue dots) model prediction for the fraction of open reaction centers (qL and qP, respectively) is plotted as a function of the fraction of open reaction centers in the multiscale simulations when the excitation diffusion length (L_D) is 50 nm (left panel), 25 nm (middle panel), and 19 nm (right panel). The corresponding multiscale simulation results fall on the diagonal of the plot, which is given as a black line for clarity.

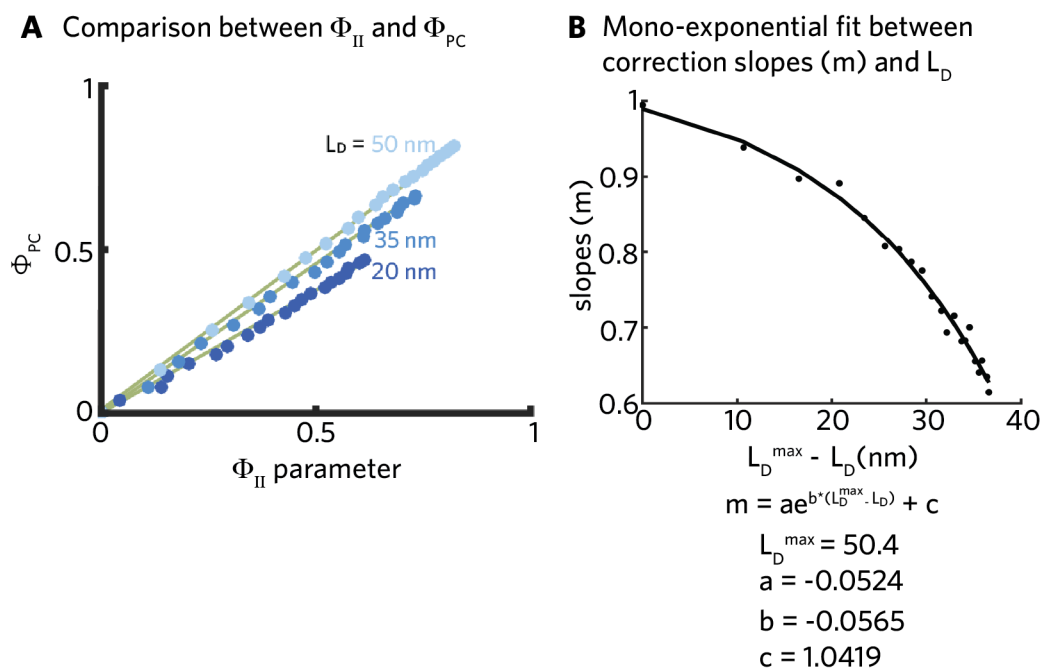


Fig. S3. Excitation diffusion length dependent correction to Φ_{II} . (A) For a given excitation diffusion length, the photochemical yield predicted using the lake/puddle models (Φ_{II}) and the multiscale model ($\Phi_{PC} = m \cdot \Phi_{II}$) have a linear relationship, as shown for three different excitation diffusion lengths (L_D) plotted in different shades of blue. (B) The pre-factor (m) which relates Φ_{II} to Φ_{PC} is plotted as a function of $L_D^{\max} - L_D$. The resulting scatter points shows a simple mono-exponential dependence. The equation describing the best fit line (black), is shown below the plot.

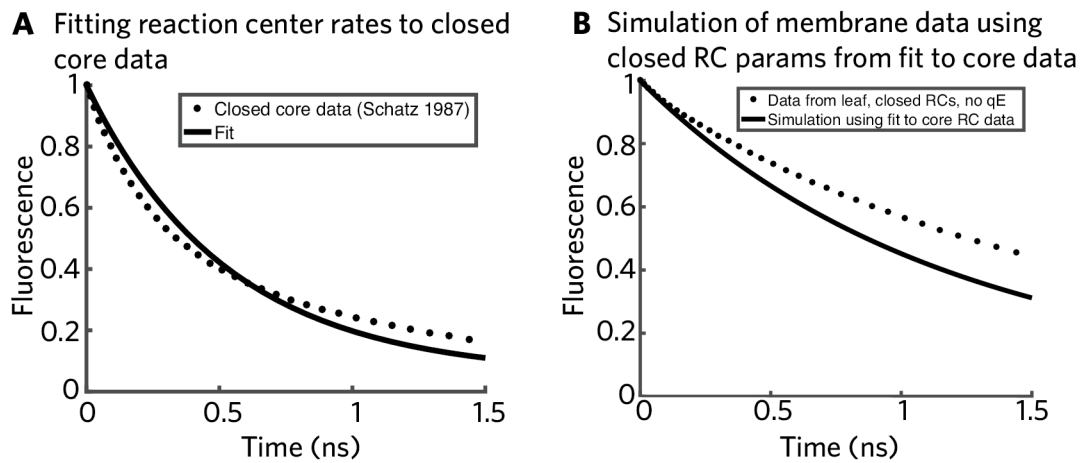


Fig. S4. Using a fit of closed reaction center rates to closed core data to simulate data from membranes with closed reaction centers and no qE. (A) Fitting the charge separation rates (eq. 3, $k_{irr} = 0$) to the fluorescence lifetime of closed PSII core complexes from Schatz, *et al.* (15). The data is indicated by the dotted line, and the fluorescence lifetime resulting from a fit of the reaction center parameters in our model to this data is indicated by the solid line. The best fit timescales to the isolated core complex for the closed RC are given by $\tau_{CS} = 125$ ps and $\tau_{RC} = 6.25$ ns (though any value $\gg 2$ ns provides an equivalent fit). (B) Using the reaction center parameters from the fit to the core in (A) in our membrane model, we simulated the fluorescence lifetime measured on a leaf with reaction centers closed and no qE by Sylak-Glassman, *et al.* (16). The data is indicated by the dotted line, and the simulation by the solid line.

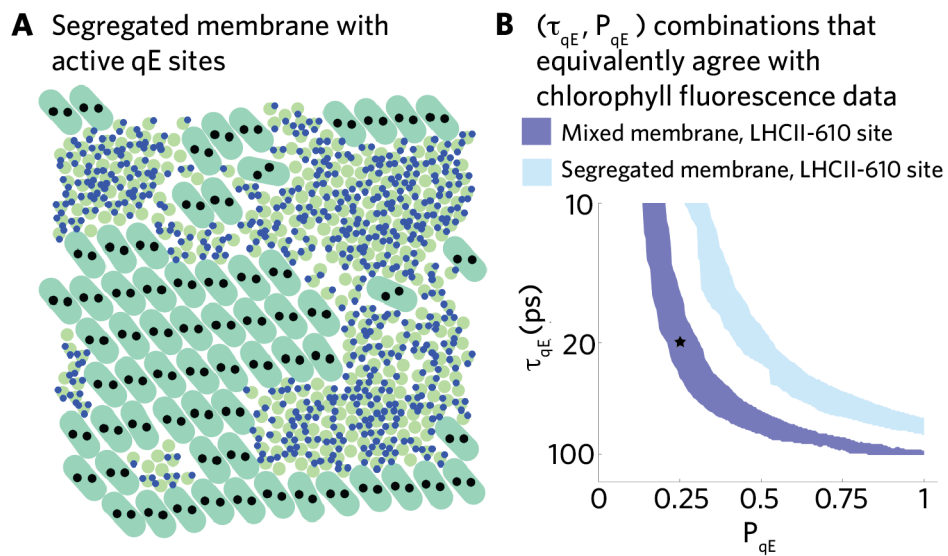


Fig. S5. Multiple (τ_{qE}, P_{qE}) combinations are consistent with fluorescence lifetime data for a spatially heterogeneous distributions of active qE sites. (A) Example of a membrane in which the LHCII (green circles) and the PSII supercomplexes (grey pills) are spatially segregated, with all reaction centers closed (black filled circles) (13). The quenching site is 610-612 domain of LHCII (LHCII-610), and activated sites are shown as filled blue dots. (B) The (τ_{qE}, P_{qE}) combinations that are consistent with the 'light acclimated' fluorescence lifetime snapshot (see SI Methods, Fluorescence lifetime snapshot data analysis for how this was determined) shown in Main Text, Fig. 2B for the LHCII-610 site in either the mixed membrane (dark blue) or the segregated membrane (light blue). The fluorescence lifetime indicated by the solid blue line in Fig. 2B of the main text is for the τ_{qE}, P_{qE} combination shown with a star. Segregation of active quenching sites (light blue) shifts such combinations to the right compared to the mixed case (blue) because of less effective quenching of excitation initiated in the PSII supercomplexes.

References

1. Schneider A, Geissler P (2013) Coexistence of Fluid and Crystalline Phases of Proteins in Photosynthetic Membranes. *Biophysical Journal* 105(5):1161–1170.
2. Caffarri S, Kouřil R, Kereiche S, Boekema EJ, Croce R (2009) Functional architecture of higher plant photosystem II supercomplexes. *EMBO J.* 28(19):3052–3063.
3. Liu Z, et al. (2004) Crystal structure of spinach major light-harvesting complex at 2.72 Å resolution. *Nature* 428(6980):287–292.
4. Kouřil R, Dekker JP, Boekema EJ (2012) Supramolecular organization of photosystem II in green plants. *Biochimica et Biophysica Acta (BBA) - Bioenergetics* 1817(1):2–12.
5. Ishizaki A, Calhoun TR, Schlau-Cohen GS, Fleming GR (2010) Quantum coherence and its interplay with protein environments in photosynthetic electronic energy transfer. *Physical Chemistry Chemical Physics* 12(27):7319–7337.
6. Raszewski G, Renger T (2008) Light harvesting in photosystem II core complexes is limited by the transfer to the trap: can the core complex turn into a photoprotective mode? *Journal of the American Chemical Society* 130(13):4431–4446.
7. Novoderezhkin V, Marin A, van Grondelle R (2011) Intra- and inter-monomeric transfers in the light harvesting LHCII complex: the Redfield–Förster picture. *Physical Chemistry Chemical Physics* 13(38):17093–17103.
8. Sumi H (1999) Theory on rates of excitation-energy transfer between molecular aggregates through distributed transition dipoles with application to the antenna system in bacterial photosynthesis. *The Journal of Physical Chemistry B* 103(1):252–260.
9. Scholes GD, Fleming GR (2000) On the mechanism of light harvesting in photosynthetic purple bacteria: B800 to B850 energy transfer. *The Journal of Physical Chemistry B* 104(8):1854–1868.
10. Bennett DIG, Amarnath K, Fleming GR (2013) A Structure-Based Model of Energy Transfer Reveals the Principles of Light Harvesting in Photosystem II Supercomplexes. *Journal of the American Chemical Society* 135(24):9164–9173.
11. Roden JJJ, Bennett DIG, Whaley KB (2016) Long-range energy transport in photosystem II. *The Journal of Chemical Physics* 144(24):245101.
12. Kreisbeck C, Kramer T, Aspuru-Guzik A (2014) Scalable high-performance algorithm for the simulation of exciton dynamics. application to the light-harvesting complex II in the presence of resonant vibrational modes. *Journal of Chemical Theory and Computation* 10(9):4045–4054.
13. Amarnath K, Bennett DIG, Schneider AR, Fleming GR (2016) Multiscale model of light harvesting by photosystem II in plants. *Proceedings of the National Academy of Sciences* 113(5):1156–1161.
14. Caffarri S, Broess K, Croce R, van Amerongen H (2011) Excitation Energy Transfer and Trapping in Higher Plant Photosystem II Complexes with Different Antenna Sizes. *Biophysical Journal* 100(9):2094–2103.
15. Schatz GH, Brock H, Holzwarth AR (1987) Picosecond kinetics of fluorescence and absorbance changes in photosystem II particles excited at low photon density. *Proceedings of the National Academy of Sciences* 84(23):8414–8418.
16. Sylak-Glassman EJ, Zaks J, Amarnath K, Leuenberger M, Fleming GR (2016) Characterizing non-photochemical quenching in leaves through fluorescence lifetime snapshots. *Photosynthesis Research* 127(1):69–76.
17. Ihalainen JA, et al. (2005) Kinetics of excitation trapping in intact photosystem I of *Chlamydomonas reinhardtii* and *Arabidopsis thaliana*. *Biochimica et Biophysica Acta (BBA) - Bioenergetics* 1706(3):267–275.
18. Schreiber U (2004) Pulse-amplitude-modulation (PAM) fluorometry and saturation pulse method: An overview. *Chlorophyll a fluorescence: A signature of photosynthesis* pp. 279–319.
19. Baker NR (2008) Chlorophyll fluorescence: A probe of photosynthesis in vivo. *Annual Review of Plant Biology* 59:89–113.
20. Brooks MD, Niyogi KK (2011) Use of a pulse-amplitude modulated chlorophyll fluorometer to study the efficiency of photosynthesis in *Arabidopsis* plants in *Chloroplast Research in Arabidopsis*. (Springer), pp. 299–310.
21. Zaks J, Amarnath K, Sylak-Glassman EJ, Fleming GR (2013) Models and measurements of energy-dependent quenching. *Photosynthesis Research* 116(2-3):389–409.
22. Kramer DM, Johnson G, Kiirats O, Edwards GE (2004) New fluorescence parameters for the determination of q_a redox state and excitation energy fluxes. *Photosynthesis Research* 79(2):209–218.
23. Robinson GW (1966) Excitation transfer and trapping in photosynthesis. in *Brookhaven Symposia in Biology*. Vol. 19, p. 16.
24. Lazár D (1999) Chlorophyll a fluorescence induction. *Biochimica et Biophysica Acta (BBA)-Bioenergetics* 1412(1):1–28.
25. Gruber JM, et al. (2016) Dynamic quenching in single photosystem II supercomplexes. *Physical Chemistry Chemical Physics* 18(37):25852–25860.
26. Duffy CDP, et al. (2012) Modeling of Fluorescence Quenching by Lutein in the Plant Light-Harvesting Complex LHCII. *The Journal of Physical Chemistry B* 117(38):10974–10986.
27. Krüger TJ, et al. (2012) Controlled Disorder in Plant Light-Harvesting Complex II Explains Its Photoprotective Role. *Biophysical Journal* 102(11):2669–2676.
28. Betterle N, et al. (2009) Light-induced dissociation of an antenna hetero-oligomer is needed for non-photochemical quenching induction. *Journal of Biological Chemistry* 284(22):15255–15266.
29. Johnson MP, et al. (2011) Photoprotective Energy Dissipation Involves the Reorganization of Photosystem II Light-Harvesting Complexes in the Grana Membranes of Spinach Chloroplasts. *The Plant Cell* 23(4):1468–1479.